Front. Earth Sci. 2020, 14(1): 50–62
https://doi.org/10.1007/s11707-019-0774-8

RESEARCH ARTICLE

Evaluating estimated sediment delivery by Revised Universal Soil Loss Equation (RUSLE) and Sediment Delivery Distributed (SEDD) in the Talar Watershed, Iran

Mohammad Saeid MIRAKHORLO, Majid RAHIMZADEGAN (✉)

Department of Water Resources, Faculty of Civil Engineering, K. N. Toosi University of Technology, Tehran, Iran

Abstract The performance of the Revised Universal Soil Loss Equation (RUSLE) as the most widely used soil erosion model is a challenging issue. Accordingly, the objective of this study is investigating the estimated sediment delivery by the RUSLE method and Sediment Delivery Distributed (SEDD) model. To this end, the Talar watershed in Iran was selected as the study area. Further, 700 paired sediment-discharge measurements at Valikbon and Shirgah-Talar hydrometric stations between the years 1991 and 2011 were collected and used in sediment rating curves. Nine procedures were investigated to produce the required RUSLE layers. The estimated soil erosion by RUSLE was evaluated using sediment rating curve data by two methods including least squares and quantile regression. The average annual suspended sediment load was calculated for each sub-watershed of the study area using the SEDD model. Afterwards, a sediment rating curve was estimated by least squares and quantile regression methods using paired discharge-sediment data. The average annual suspended sediment load values were calculated for two hydrometric stations and were further evaluated by the SEDD model. The results indicated that the first considered procedure, which utilized 15-min rainfall measurements for the rainfall factor (R), and the classification method of SENTINEL-2 MSI image for the cover management factor (C), offered the best results in producing RUSLE layers. Furthermore, the results revealed the advantages of utilizing satellite images in producing cover management layer, which is required in the RUSLE method.

Keywords Revised Universal Soil Loss Equation (RUSLE), sediment rating curve, quantile regression, Geographic Information System (GIS)

1 Introduction

Soil erosion in watersheds and sedimentation in rivers, creek waters, farmlands, and reservoirs are among the main concerns for farmers and relevant managers on both local and global scales (Dregne, 1992; Zounemat-Kermani et al., 2016; Wei et al., 2017). Further, soil erosion causes problems in mega-rivers all over the world. For instance, Dai et al. (2015) investigated the Anthropocene risk of soil erosion in the Changjiang submerged delta due to the impacts of the Three Gorges Dam (TGD), the world's largest dam. Their results indicated a rate of accumulation as high as 10 cm/yr at the depocenter of the submerged delta between 1958 and 2009. Further, Mei et al. (2018) proved that the extensive erosion of the natural floodplain of TGD compromised the full beneficial impact of floodwater retention by this dam. Dai et al. (2016) studied the decline of the suspended sediment concentration delivered by the Changjiang (Yangtze) River into the East China Sea between the years 1956 and 2013. According to them, the large-scale soil erosion in the 1950s can be the reason for this reduction. Hassan et al. (2017) analyzed the contemporary patterns of fluvial sediment delivery in the Mississippi River basin. They assessed the impact of the regional land conditions on variations in the sediment delivery within the basin. They proved that the recent sediment is sourced primarily along the river valleys from arable lands, stream banks, and channel erosion. Furthermore, based on Iikhchi et al. (2003), the mean yearly erosion in Iran is about 4.3 times greater than that across the world.

Although it is possible to instrument a few individual watersheds to perform measurements for evaluating soil erosion and sediment delivery, one cannot study every single location in detail. Instead, application of models to assess this problem can be useful (Morgan and Nearing, 2016). Sediment delivery indicates the amount of sediment

Received November 10, 2018; accepted May 21, 2019

E-mail: rahimzadegan@kntu.ac.ir

produced by soil erosion and exported from each watershed or subwatershed. Numerous models have been developed to calculate the soil erosion/sediment delivery. Each of these models has had different efficiencies in various watersheds with different climates. The soil erosion models can be classified into three main categories: 1) empirical models, 2) physical-based models, and 3) conceptual models (Mirakhorlo and Rahimzadegan, 2018).

Wischmeier and Smith (1978) developed USLE as one of the most practical soil erosion models. Renard et al. (1997) developed RUSLE which predicts long-term average annual soil loss caused by raindrop splash and runoff from specific field slopes in special cropping and management systems and from the rangelands. The RUSLE model provided in the United States Agricultural handbook 703 uses six factors including rainfall-runoff erosivity, soil erodibility, slope length, slope steepness, cover-management, and support practices (Renard et al., 1997).

The procedures based on Geographic Information System (GIS) can be used to determine effective factors on the soil erosion in a cell via RUSLE (Renard et al., 1997). The benefits of using GIS in the environmental assessment were first reported by Eedy (1995). Also, Vrieling (2006) explained the application of Remote Sensing (RS) for the soil erosion assessment.

Different procedures have been used in the literature to calculate soil erosion by USLE/RUSLE. Lee and Kang (2014) estimated sediment delivery based on RUSLE, SEDD, and the observational data in a watershed in South Korea. They attempted to estimate sediment delivery based on the observed data in the monsoon region of South Korea. Fathizad et al. (2014) employed RUSLE in a semi-arid watershed in Iran and estimated 7.96% greater sediment delivery as compared to the measured data. Tanyaş et al. (2015) implemented RUSLE and SEDD while introducing an innovative method to assess the cover-management factor in a basin in Turkey. They assessed sediment delivery by bathymetry of the reservoir. Fernández and Vega (2016) applied RUSLE and PAN-European Soil Erosion Risk Assessment (PESERA) in the north-west of Spain and compared the results of the two models. They concluded that the PESERA results were more precise than those from the other two models. Mondal et al. (2018) investigated the results acquired from three soil erosion models including Morgan-Morgan-Finney (MMF), USLE, and RUSLE using GIS platform. Their study area was a part of Narmada River in the Central India. They found RUSLE as the most reliable model for the study area. Mirakhorlo and Rahimzadegan (2018) implemented EPM and MPSIAC models in the Talar watershed, Iran. They evaluated the results of the soil erosion models by the sediment rating curve (SRC) model. They proved the better performance of MPSIAC compared to EPM.

Different methods have been used in previous studies to produce the RUSLE factors, but the performance and underlying processes of the methods have been different. Therefore, the main objective of this study was investigating RUSLE-based soil erosion maps regarding sediment delivery. It was accomplished using nine different procedures to create base maps using RS and GIS. For this purpose, Talar watershed in Iran was selected as the study area. A sediment delivery map was provided for each sub-watershed of the study area using SEDD. Further, a quantile regression method was utilized to estimate the suspended sediment load for two stations at the end of the watershed with the results compared with acquired sediment delivery of SEDD. The differences between considered approaches and their impacts in estimating soil erosion/sediment delivery maps were investigated by RUSLE and SEDD.

2 Materials and methods

2.1 Study area

Talar watershed in Iran was selected to implement the proposed methods of this study and to evaluate the results. This watershed is located from 52°35′22.2″E to 53°23′34.19″E eastern longitude and from 35°44′23.06″N to 36°19′1.6″N northern latitude. Talar watershed is drained by the main Talar River which extends from south to north (Fig. 1). The main Talar River is 100 km long and intersects the Kassilian River. The total area of the watershed is about 210088 ha. The higher elevations are located in the north-west extremes reaching 3910 m in height, and the lowest elevation is located at the end point of the watershed in the north, with a height of 215 m above the mean sea level.

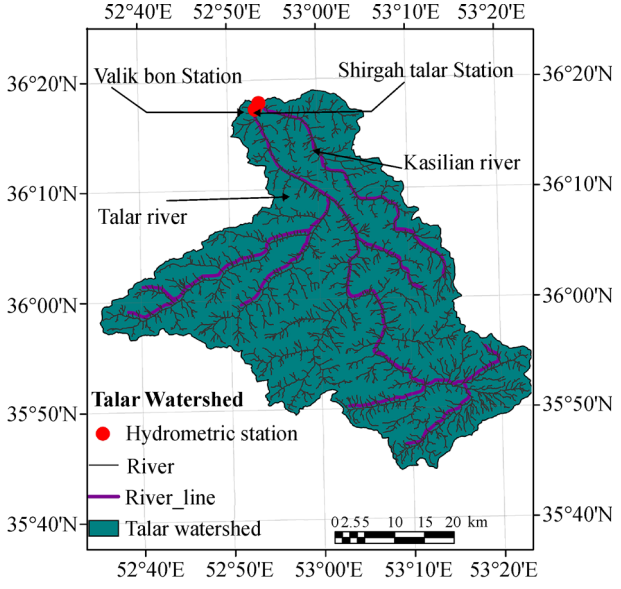

Fig. 1 Location of the study area and the utilized hydrometric stations.

2.2 Data used

In this study, data from rainfall stations (Fig. 2), including 15 min rainfall data from 10 stations and monthly rainfall data from 8 stations, were used. Valikbon and Shirgah-Talar Hydrometric stations data (Fig. 2) were used as well to validate the yearly suspended sediment load estimation. The data included about 700 paired suspended sediment-discharge recorded measurements for each station, along with 20-year discharge data recorded between years 1991 and 2011. The bed sediment load values were not available. Further, the information of the soil and land capability report was also utilized as provided by The Ministry of Agriculture of Iran. Meanwhile, Shuttle Radar Topography Mission Digital Elevation Model (SRTM DEM) data acquired in 2007 with 30 m spatial resolution was obtained from USGS website and utilized further. In addition, a SENTINEL-2 Multi-Spectral Instrument (MSI) image acquired on June 06, 2017 was acquired from Copernicus website and was used to produce the cover management factor.

2.3 Methodology

2.3.1 RUSLE model

RUSLE model quantifies soil erosion based on six factors:

$$A = R \times K \times L \times S \times C \times P, \tag{1}$$

where A is the soil loss per unit of area $(t/(\text{ha}\cdot\text{yr}))$, R denotes the rainfall-runoff erosivity factor $((\text{Mj}\cdot\text{mm})/(\text{ha}\cdot\text{h}\cdot\text{yr}))$, K is the soil erodibility factor $((\text{Mj}\cdot\text{mm})/(\text{ha}\cdot\text{h}\cdot\text{yr}))$, L refers to the slope length factor, S is the slope steepness factor, C shows the cover-management factor, and P denotes the support practice factor. In this study, R factor was calculated in three ways and C factor was estimated using three methods. Then, nine soil erosion maps were produced using nine procedures, and were imported into the SEDD model (Fig. 3).

2.3.1.1 R factor

In this study, three frequently used equations have been considered to calculate the R factor. The first equation was proposed by Wischmeier and Smith (1978) as:

$$R = \frac{1}{n}\sum_{j=1}^{n}\left[\sum_{k=1}^{m}(E)(I_{30})_k\right], \tag{2}$$

where I_{30} denotes the maximum 30 min rainfall intensity, j shows the number of years used to produce the average, k is the numbers of storms in each year, n denotes the number of years used to obtain average R, and m is the number of storms in each year. Also, E is the total storm kinetic energy. Note that the precipitation rate, which is less than 12.7 mm in 30 min or 6.34 mm in 15 min, was eliminated from the erosion index calculation (Renard et al., 1997).

One of the problems which appears in studies on watersheds is the lack of 30 min or 15 min data. Accordingly, another equation proposed by Renard and Freimund (1994) to estimate the R factor, which uses the monthly rainfall data, was applied as the second equation:

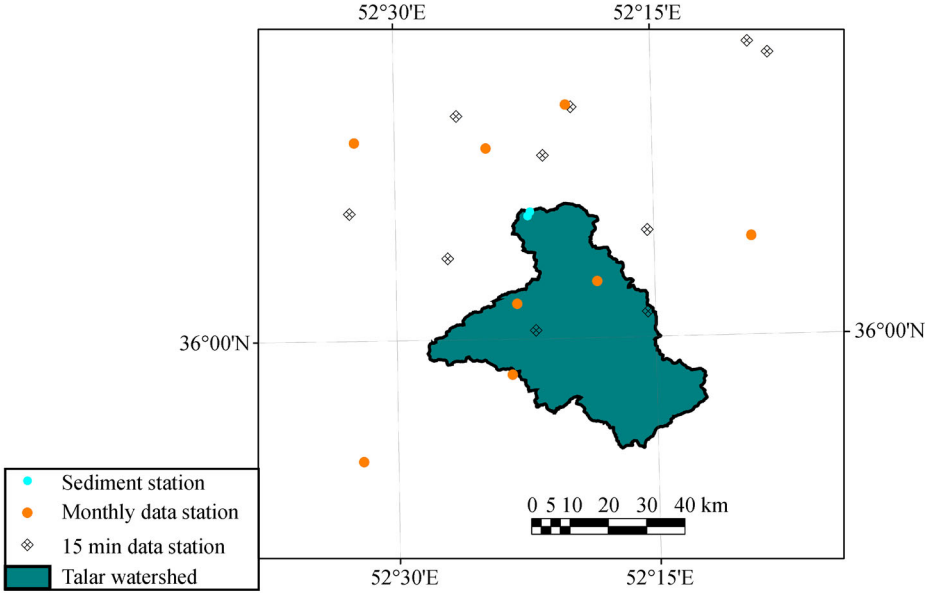

Fig. 2 Distribution of the utilized rainfall stations in the study area.

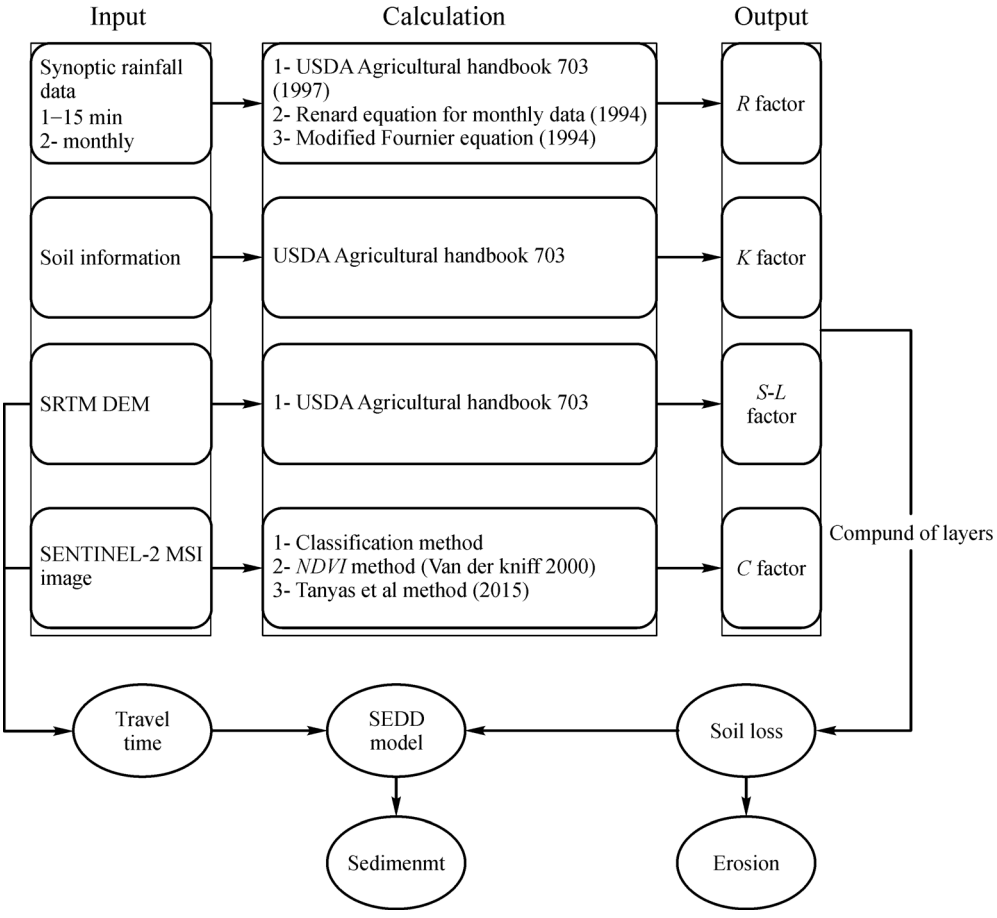

Fig. 3 The flowchart for soil erosion/sediment delivery calculation utilized in this study.

$$\begin{cases} R = 0.0483Pr^{1.610} & Pr < 850 \text{ mm} \\ R = 587.8 - 1.219Pr + 0.004105Pr^2 & Pr \geqslant 850 \text{ mm} \end{cases}, \quad (3)$$

where Pr is the mean yearly rainfall (mm).

Meanwhile, an equation based on the modified Fournier index for watersheds with insufficient information was used as the third equation (Renard and Freimund, 1994):

$$\begin{cases} R = 0.07397F^{1.847} & F < 55 \text{ mm} \\ R = 95.77 - 6.081F + 0.4770F^2 & F \geqslant 55 \text{ mm} \end{cases}, \quad (4)$$

where F is modified Fournier index as:

$$F = \sum_{i=1}^{12} \rho_i^2 / P, \quad (5)$$

where ρ_i and P represent the mean monthly rainfall and the mean yearly rainfall, respectively.

Note that the R factor was calculated for the locations of the stations. Meanwhile, interpolation methods must be used in order to generate the map of R factor. The circular-ordinary Kriging interpolation method was utilized in this study.

2.3.1.2 K factor

The K factor captures the effect of soil properties and the characteristics of the soil profile on soil loss. The best way to calculate the K factor is using a nomograph. A useful algebraic approximation of the nomograph, for the cases where the silt fraction does not exceed 70%, was proposed by Wischmeier and Smith (1978) and also used in this study.

2.3.1.3 S and L factors

S and L factors represent the effect of topography on soil erosion. Both factors can be calculated by DEM. In the RUSLE model, slope length is as follows:

$$L = (\lambda/22.128)^m, \quad (6)$$

where λ is the pixel length (m) (Renard et al. 1997). Also, m shows the slope length exponent related to the ratio of rill erosion to inter-rill erosion (Renard et al. 1997). The slope steepness factor *(S)* is evaluated by:

$$\begin{cases} S = 10.8\sin\theta + 0.03 & s < 9\% \\ S = 16.8\sin\theta - 0.50 & s \geqslant 9\% \end{cases}, \quad (7)$$

where s shows the slope for each pixel.

2.3.1.4 *C* factor

Different methods have been proposed to calculate the *C* factor. The main equation proposed by Renard et al. (1997) consists of 5 sub-factors:

$$SLR = PLU \times CC \times SC \times SR \times SM, \quad (8)$$

where *SLR* is the soil-loss ratio for the given condition, *PLU* denotes the prior-land-use sub-factor, *CC* is the canopy-cover sub-factor, *SC* shows the surface-cover sub-factor, *SR* is the surface roughness sub-factor, and *SM* denotes the soil-moisture sub-factor. The *C* factor is calculated as:

$$C = \sum_{i=1}^{n} SLR_i EI_i / EI_t, \quad (9)$$

where SLR_i is the value for the ith time period, EI_i denotes the percentage of the annual storm erosivity factor (*EI*) occurring during that time period, n is the number of periods used in the summation, and EI_t refers to the sum of the *EI* percentages for the entire time period (Renard et al., 1997). Calculation of this equation requires massive information for producing the sub-factors, while the accuracy is not high enough using insufficient samples. Therefore, to calculate the *C* factor, it is not possible to use this approach. Hence, three methods as mentioned further were used to calculate the *C* factor in this study (Fig. 4).

In the first method, a satellite image is classified into land-use classes, where the *C* factor values are assigned to each land-use class. To evaluate the classified satellite images and to choose the best classification method, the overall accuracy and the kappa coefficient could be used. One drawback of this method is that gradual changes are not considered and the *C* factor is fixed for each class.

The second method utilizes the Normalized Differences Vegetation Index (*NDVI*) on the satellite images and imposes an empirical equation to calculate the *C* factor. Based on Van der Knijff et al. (2000), the relation of *NDVI* and the monthly *C* factor is:

$$\begin{cases} C = \exp\left(-\alpha \dfrac{NDVI}{\beta - NDVI}\right) & NDVI > 0 \\ C = 1 & NDVI \leqslant 0 \end{cases}, \quad (10)$$

where it is assumed that $\alpha = 2$ and $\beta = 1$ to acquire reasonable results.

In the third method, which was proposed by Tanyaş et al. (2015), *C* factor for each pixel is:

$$C_{\text{raw}} = PLU \times VD \times TWI \times TRI, \quad (11)$$

where C_{raw} is the raw value of the *C* factor, *PLU* denotes the prior land-use, *VD* represents vegetation density which is equivalent to the *CC* and *SC* sub-factors. Also, *TWI* is considered as an indicator for *SM* and *TRI* refers to *SR*.

PLU represents the influence of former crop and tillage practices on soil erosion which can be calculated based on the surface-soil-consolidation factor (C_f). In this study, C_f values and consequently *PLU* values were determined using a land-use map.

In Eq. (11), *VD* is equivalent to *CC* and *SC* data layers.

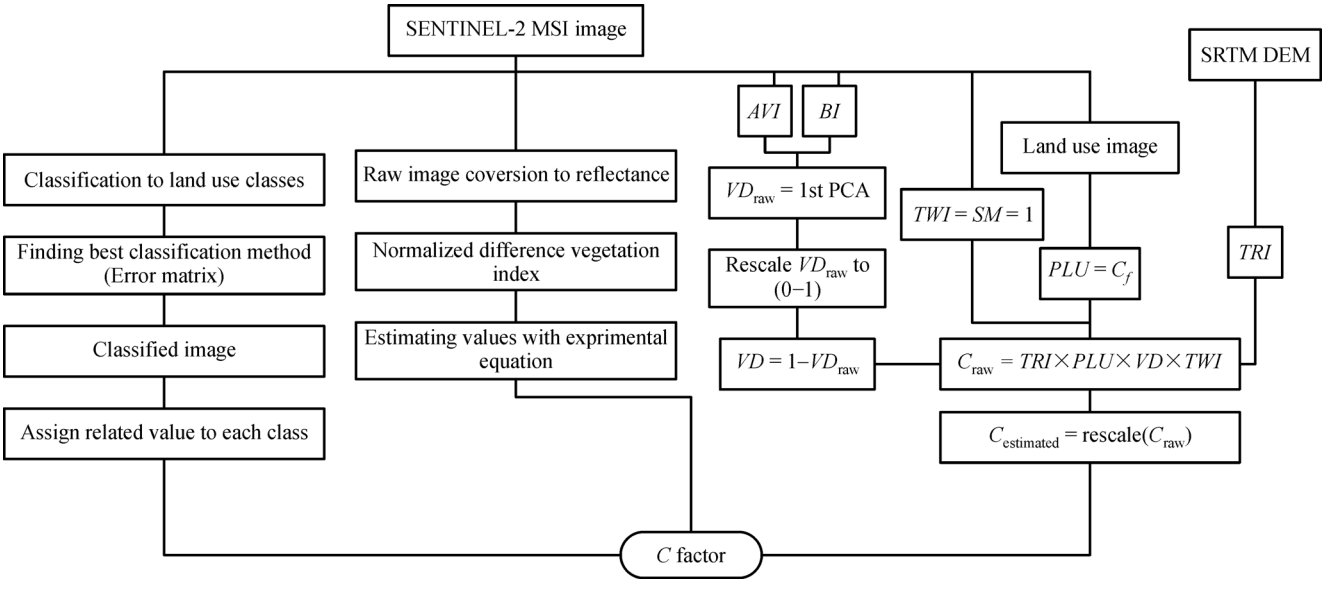

Fig. 4 Flowchart of the calculation of the *C* factor using the proposed procedures.

To determine *VD*, Advanced Vegetation Index (*AVI*) and Bareland Index (*BI*) were initially calculated. *AVI* is more dependent on the vegetation density and can be determined as:

$$\begin{cases} AVI = [(B5+1)\times(256-B4)\times(B5-B4)]^{1/3} & B4 < B5 \\ AVI = 0 & B4 \geqslant B5 \end{cases}, \tag{12}$$

where B_i corresponds to MSI bands.

BI is proposed to distinguish vegetation from the background under different conditions, and can be calculated as:

$$BI = \frac{(B11+B4)-(B5+B1)}{(B11+B4)+(B4+B1)} \times 100 + 100. \tag{13}$$

Then, VD_{raw} index, which represents the primary values of the *VD* index, is estimated by principle component analysis (PCA) of AVI and BI. Finally, to achieve normalized *VD* (ranging 0 to 1) and compatibility with the other parameters, VD_{raw} values have been subtracted from 1.

To calculate soil moisture, the topographic wetness index *(TWI)* based on Beven and Kirkby (1979) was utilized. The terrain roughness index (TRI) proposed by Riley et al. (1999) was employed to calculate surface roughness. *TRI* calculates the mean differences between the value of a pixel and its eight neighboring pixels, which represent *SR*. Eventually, C_{raw} factor was obtained by multiplying the layers. However, based on Tanyaş et al. (2015), C_{raw} is not congruent with experimental based C factor. Therefore, C_{raw} values should be rescaled into specific ranges of *C* factor. An *NDVI*-based procedure for estimating *C* (Van der Knijff et al., 2000) is a suitable method to specify these ranges. Using this procedure, the corresponding *C* values to upper and lower *NDVI* values of each class can be achieved (Tanyaş et al., 2015).

2.3.1.5 *P* factor

P factor is the ratio of soil loss with a specific support practice to the corresponding loss with up- and down-slope tillage (Wischmeier and Smith, 1978). Different *P* factors are used for contour strip-cropping and terracing given the slope length and gradient. In this study, due to the lack of conservation practices to control soil erosion, the *P* factor was assumed to be one.

2.3.2 SEDD model

In the SEDD model, the sediment production Y_i for each pixel *i* of the basin is defined as follows (Ferro and Porto, 2000):

$$Y_i = SDR_i \times A_i \times SU_i, \tag{14}$$

where A_i is soil loss (t/ha) from pixel *i*, SU_i shows the area (ha) of the pixel, and SDR_i denotes sediment delivery ratio. SDR_i depends on travel time $t_{p,i}$ of the eroded particles along the hydraulic path, from the desired pixel to the nearest stream pixel (Mirakhorlo and Rahimzadegan, 2018):

$$SDR_i = \exp(-\beta t_i), \tag{15}$$

where β is a coefficient (Yang et al., 2012).

Ferro and Minacapilli (1995) expressed that the sediment delivery equation is independent of the selected soil erosion model and can be estimated using only morphological data:

$$SDR_w = \frac{\sum_{i=1}^{N} \exp(-\beta t_i)\lambda_i^{0.5} s_i^2 S_i}{\sum_{i=1}^{N_u} \lambda_i^{0.5} s_i^2 S_i}, \tag{16}$$

where *N* is the total number of cells over the watershed, λ_i is the length of cell *i* along the flow path, s_i denotes the slope of the cell, and S_i refers to the area of the cell (Minacapilli and Santoro, 2003).

2.3.3 Sediment rating curve method

Due to the lack of paired sediment-discharge data in two hydrometric stations located at the two ends of the study area, the SRC method was used to estimate the average annual Suspended Sediment Load (SSL). The SRC signifies the empirical relationship between measured SSL and discharge. The relationship between these two parameters is often expressed by a power function. Then, a sequence of daily SSL can be estimated using obtained SRC and daily discharge series. The cumulative SSL over a longer period, such as a month or a year, is calculated as the sum of daily SSL during that time period:

$$L_n = \sum_{i=1}^{n} \hat{Q}_{s,i} = \sum_{i=1}^{n} aQ_i^b, \tag{17}$$

where L_n is the cumulative SSL during an *n* day period, $\hat{Q}_{s,i}$ shows the estimated SSL of the *i*th day via SRC, Q_i present the *i*th day discharge, and *n* shows the number of days (Shiau and Chen, 2015).

According to the small number of measurements during high discharge periods, SSL estimation produced by an SRC for such periods generally leads to greater errors. Then, a method should be used to model uncertainty along with an accurate SSL estimation in water resources planning and management (Shiau and Chen, 2015). One option to estimate the daily and monthly SSL is using the quantile regression (QR) method, as first proposed by Koenker and Bassett (1978). QR is a statistical approach for regression on different quantiles instead of regression

only on the mean. QR equation is based on the power law. The SRC for different quantiles is expressed as below (Shiau and Chen, 2015):

$$Q_{s,q} = a_q Q^{b_q}, \tag{18}$$

where q represents qth quantile (between 0 and 1), which shows probability, and $Q_{s,q}$ denotes a conditional SSL at quantile q given a discharge of Q. The coefficients a_q and b_q represent quantile-dependent regression coefficients specified by the selected quantile q and minimizing the sum of asymmetrically weighted absolute deviations as follows (Shiau and Chen, 2015):

$$\min\left[\sum_{i:Q_{s,i}\geq a_q Q_i^{bq}} q|Q_{s,i}-a_q Q_i^{b_q}| + \sum_{i:Q_{s,i}<a_q Q_i^{bq}} (1-q)|Q_{s,i}-a_q Q_i^{b_q}|\right]. \tag{19}$$

2.3.4 Estimation of the probability distribution of annual SSL

The conditional SSL $\hat{Q}_{s,q}$ for each quantile-dependent SRC is calculated by setting 20 years (1991–2011) of daily discharge as Q. The conditional SSL $\hat{Q}_{s,q}$ along with quantile q creates an estimated cumulative probability function (CDF) for the daily SSL. In this study, SSL was considered as a discrete random variable. Afterwards, the empirical probability mass function (PMF) was constructed using the obtained CDF. Finally, annual SSL was calculated using convolution theorem (Shiau and Chen, 2015). All of these processes were performed using the R programming language and "quantreg" package developed by Koenker (2012).

3 Results and discussion

3.1 RUSLE model

3.1.1 *R* factor layer

The *R* factor map was obtained using three mentioned methods including 15 min data according to Wischmeier and Smith (1978) (Fig. 5(a)), monthly data using methods of Renard and Freimund (1994) (Fig. 5(b)), and modified Fournier (1960) equation (Fig. 5(c)). Due to the differences in the locations of 15 min and monthly stations, the acquired values for *R* factor maps show different distributions. However, the second and third mentioned methods demonstrated a similar pattern of R map as they applied the same data set (monthly data). Further, the *R* factor values for 15 min stations possess a far wider range compared with monthly stations. The reason is that the 15 min data can reveal the deviations more accurately, but these extremes may be eliminated in the monthly data. In the regions lacing 15 min rainfall data, the map of R factor can be generated by the second and third methods using monthly rainfall data. However, some detailed rainfall events may be missed in the second and third methods of this study to produce the maps of *R* factor.

In this study, use of interpolation methods may cause some uncertainties in the produced *R* factor maps. This is due to major elevation fluctuations in the utilized rainfall stations in the area of study and the lack of enough stations across different elevation ranges.

3.1.2 *K* factor layer

To produce the soil erodibility factor layer, the corresponding values for each soil type, extracted from the soil capability report of Agriculture Ministry of Iran, were determined and the final map was generated (Fig. 6(a)).

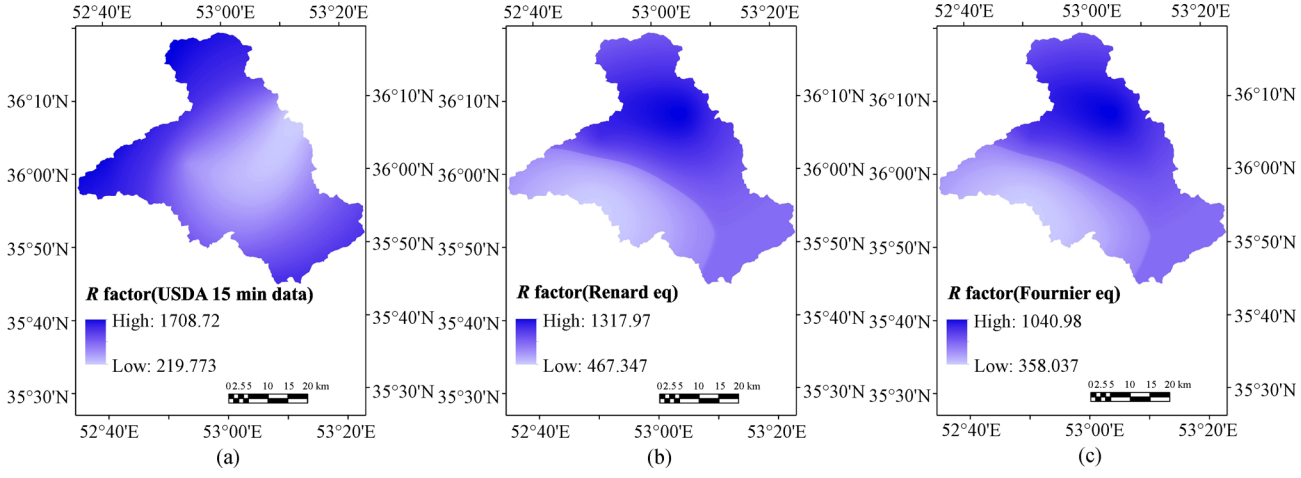

Fig. 5 *R* factor maps based on (a) USDA 703, (b) Renard equation, and (c) modified Fournier equation.

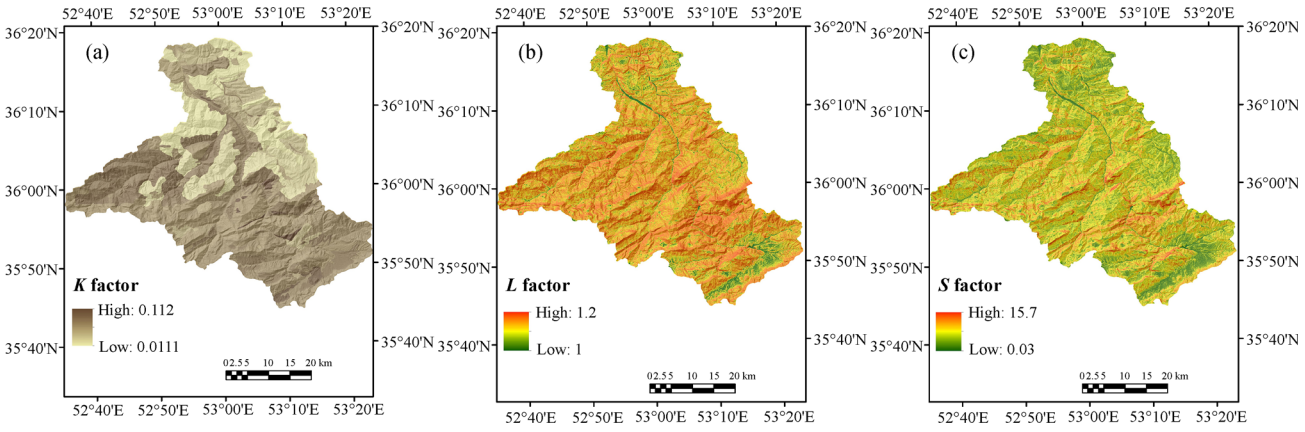

Fig. 6 Produced maps of (a) *K* factor, (b) *L* factor, and (c) *S* factor.

3.1.3 *C* factor

The *C* factor map was produced using the three mentioned methods, which apply the prepared MSI image. In the first method, the MSI image was classified using three methods including maximum likelihood, neural network, and support vector machine (SVM). Among those classification methods, SVM was chosen as the best method (with an overall accuracy of 86.63% and Kappa coefficient of 0.84, which led to the minimum error). Table 1 presents the *C* factors assigned to different land-uses from similar studies. In this method, the minimum *C* factor (0.005) was assigned to the dense-forest land-use, which had the greatest impact on preventing splashing rain. The maximum *C* value (1) was attributed to the bareland class, representing lands with a poor vegetation cover. Meanwhile, the *C* values for the settlement and road classes were equal to zero due to the lack of erosion in these classes (Fig. 7(a)).

In the second method, the equation proposed by Van der Knijff et al. (2000) was employed via *NDVI* (Fig. 7(b)). In this method, unlike the previous method, the gradual changes have been illustrated.

In the third method, *AVI* and *BI* were calculated initially using the MSI image. Then, the VD_{raw} values were obtained with the first PCA, and eventually *VD* was produced within the range of 0–1 by normalizing the VD_{raw}. Due to high humid conditions and saturation of the soil in the Talar watershed, *TWI* sub-factor can be considered as 1. To generate *PLU* according to the land-use classes, the value considered for the land-use classes of dense forest and degraded forest was 0.45, while for the settlement and road classes it was 0, while for the other classes the value was 1. Furthermore, *TRI* was calculated and normalized as SR. Then, C_{raw} for each pixel was calculated using the acquired layers. Finally, to produce the *C* map ($C_{\text{estimated}}$), C_{raw} values were rescaled to C_{NDVI} values based on different *NDVI* values in each land-use class (Fig. 7(c)).

3.2 Discussion on RUSLE and SEDD models

The soil erosion maps were generated by combining the acquired layers for procedures 1 to 9 (Figs. 8(a) –8(i)). The maximum soil erosion in the pixel unit among all of the procedures was acquired as 227.378 t/y·ha using the first procedure.

To implement the SEDD model, the Talar watershed was initially divided into 42 sub-watersheds as the SEDD model has been validated only for watersheds with areas less than 70 km^2 (Minacapilli and Santoro, 2003). Then, SDR_w values for each sub-watershed were calculated. Afterwards, β was calculated based on Eq. (16), after which the sediment delivery ratio for each pixel was calculated using Eq. (15). Finally, to evaluate the sediment delivery for each sub-watershed, the sum of the estimated sediment deliveries for all erosion layers in each sub-watershed was calculated based on the considered nine procedures (Figs. 9(a)–(i)).

According to Fig. 9, sediment delivery values in sub-watersheds in the northern part were lower due to the less steep topography and the greater vegetation cover. In the

Table 1 *C* factor values assigned to each land-use

Class	*C* factor	Percent of area	Class	*C* factor	Percent of area
Forest	0.005	32.41	Settlement	0	0.36
Degraded Forest	0.5	19.22	Bareland	1	38.23
Pasture	0.25	3.51	Road	0	0.88
Farmland	0.3	5.387			

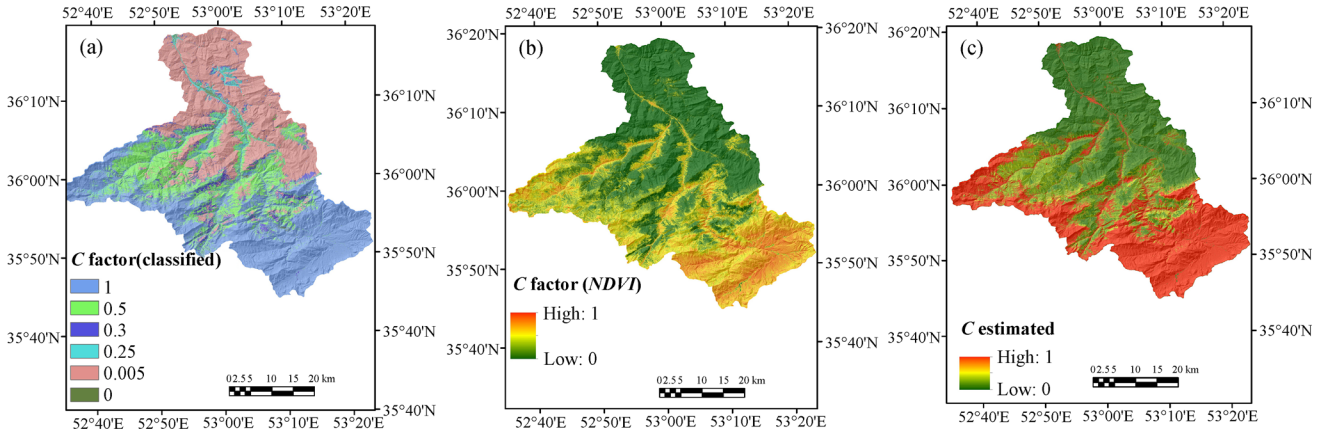

Fig. 7 The *C* factor map for Talar watershed based on (a) Land-uses, (b) Van der Knijff et al. (2000), and (c) Tanyaş et al. (2015).

sub-watersheds of the southern and western parts, sediment delivery values were far greater than in northern sub-watersheds. However, the sediment delivery ratio for each sub-watershed was different depending on the selected procedure.

Measurements at Valikbon and Shirgah-Talar stations were used to produce the average annual suspended sediment load using regression equations for evaluating the acquired SSL values. Hence, annual SSLs for Valikbon and Shirgah-Talar stations were obtained using 20-year data of discharge (1992–2011) (Figs. 10 and 11). Note that the produced SSLs at Valikbon station was formed by sub-watersheds 1, 2, 3, 5, 7, 9, and 15. The rest of sub-watersheds were related to the major Talar River, with the SSLs measured in Shirgah-Talar station corresponding to those sub-watersheds.

Figures 10 and 11 display the estimated SSL for Shirgah-Talar and Valikbon stations, respectively. The box plot reveals the minimum (first percentile), first quartile, median (second quartile), third quartile, and the maximum (99th percentile) estimation of annual SSL based on QR. Red dots represent yearly SSL produced by the least squares method. Horizontal blue lines indicate the estimated cumulative average annual sediment deliveries for sub-watersheds entering the considered stations. These values were estimated by the SEDD model for the desired P1 to P9 procedures. As observed in Figs. 10 and 11, estimation of yearly SSL for different years has a great uncertainty. Differences between the QR method and the least squares method in estimation of yearly SSL suggest uneven dispersal of information. It means that the method of least squares tries to minimize errors and to estimate SRC based on the mean value, but the estimated curves in QR are based on different quantiles.

As Fig. 10(b) shows, the interquartile for the mean ranges from 713 to 840 $\times 10^3$ tons indicating that the most likely mean annual SSL with probability of 0.5 occurs within this range. Further, procedure 1 leads to the best results for Shirgah-Talar station. This procedure used 15 min data and the USDA 703 equation to calculate the *R* factor. This can be due to use of 15 min data with the detailed information about the effect of raindrop impact. On the other hand, the classification method was used to produce the *C* factor layer in procedure 1. This can prove the efficiency of using the classification method on satellite images to produce the *C* factor.

Based on Fig. 11, for Valikbon station, the most probable range of the mean has been 3.142×10^3–3.702×10^3 tons (Fig. 11(b)), but none of the procedures lied within this range. The maximum value of the average annual SSL occurred in P7 case. This procedure led to the best result compared to the other procedures based on QR-estimated SSL. Note that the difference between the results acquired from the SEDD model and estimated yearly SSL based on observed data in this station has been far less. An important reason for the low estimated sediment delivery by the SEDD model in this station could be high vegetation cover and *C* factor influence. Another important reason can be the lack of sediment data in the estimation of SRC for calculations.

In general, it can be concluded that P1 has the best performance compared to the other procedures for the two hydrometric stations. The reason is that most of the outlet of the Talar watershed feeds to the Shirgah-Talar watershed. Another reason includes the closer result of this procedure to the mean yearly value and most likely average annual SSL regarding to Fig. 10. On the other hand, estimated SSL for this station was far greater than for Valikbon station (about 100 times greater values in the observed SSL).

The results proved the better performance of P1 compared to EPM and MPSIAC models, which were previously implemented by Mirakhorlo and Rahimzadegan (2018) for the Talar watershed. This can be inferred from the results acquired at the Shirgah-Talar watershed as the major outlet feed of the Talar watershed. Nevertheless, at the Valikbon station, EPM suggested a better performance compared to all of the nine proposed procedures.

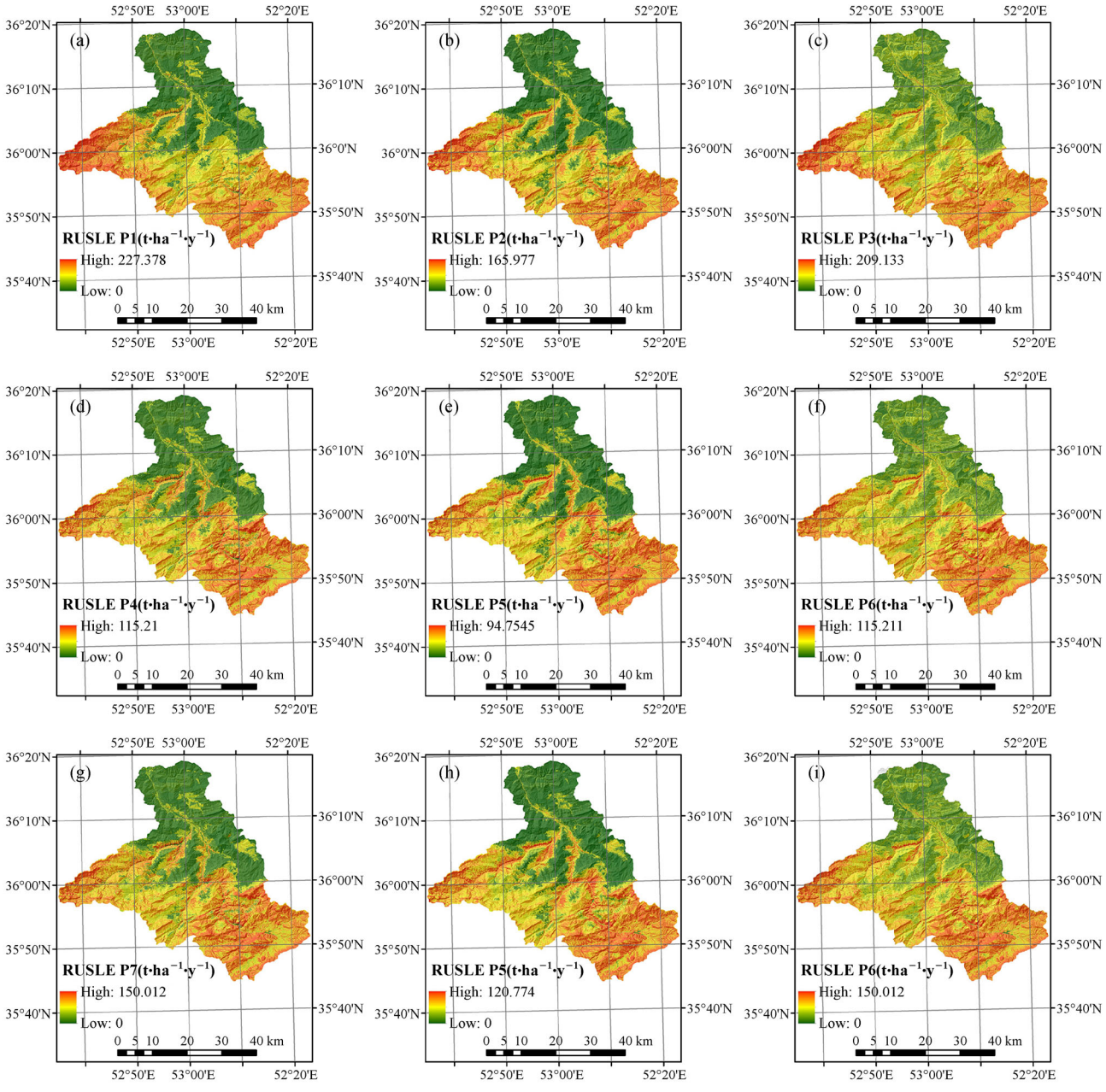

Fig. 8 Produced soil erosion maps by procedures 1 to 9.

4 Conclusions

Although the RUSLE model is one of the most widely used models to assess soil erosion in watersheds, the accuracy of the achieved results is often ambiguous. This is due to the lack of adequate soil loss-SSL data or the inappropriate performance of soil erosion-sediment delivery models. Accordingly, nine procedures were implemented in this research to generate soil loss and sediment delivery using RUSLE for the Talar watershed in GIS. For the rainfall-runoff erosivity factor layer of RUSLE (*R*), three different methods were used, and to produce the cover-management factor of RUSLE (*C*), three different methods of analysis were applied on a SENTINEL-2 MSI image. Further, in order to produce the average annual sediment delivery in each sub-watershed, the SEDD model was applied on nine produced soil erosion maps. Due to insufficient SSL data, SRCs created by QR method were employed to evaluate the results.

The results of the soil erosion maps and sediment delivery revealed that the trends of changes in different locations were similar. However, regarding the soil erosion and sediment delivery values, considerable differences were observed in each subwatershed and the whole study

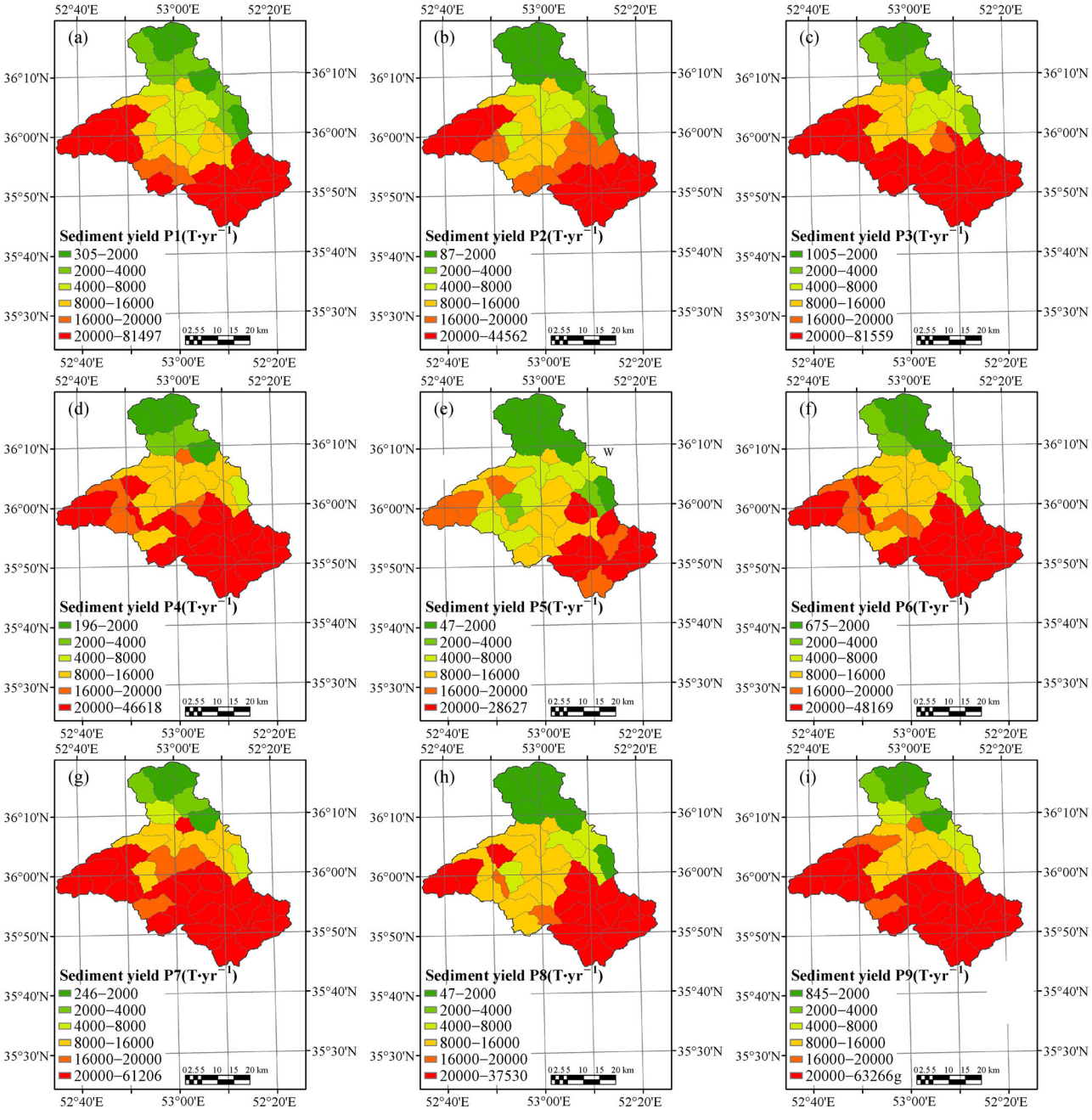

Fig. 9 Eroded sediment delivery of sub-watersheds based on the procedures P1 to P9 (a–i).

area. According to the obtained maps, it can be concluded that in southern and western areas of the Talar watershed, where vegetation cover was lower and had steeper slopes, higher values of soil erosion were predicted. Differences between the procedures used to estimate soil erosion led to soil erosion maps with different spatial distributions. This indicated that use of monthly and 15 min data can create major differences in the estimation of soil erosion. On the other hand, the number of stations and the spatial distribution of the stations affect the validation of the results. Furthermore, the interpolation method used for different stations can affect the *R* factor map. However, based on the obtained results, application of the USDA 703 approach with 15 min data was the best procedure to calculate the *R* factor, if enough information was available. To calculate *C* factor, the method based on the definition of a fixed value for each land-use class led to a soil erosion map with a unique value for a specific land-use. The procedure based on NDVI underestimated the *C* factors compared to other methods. Conversely, the method presented by Tanyaş et al. (2015) overestimated the *C* factor. Further, this method had a greater compatibility

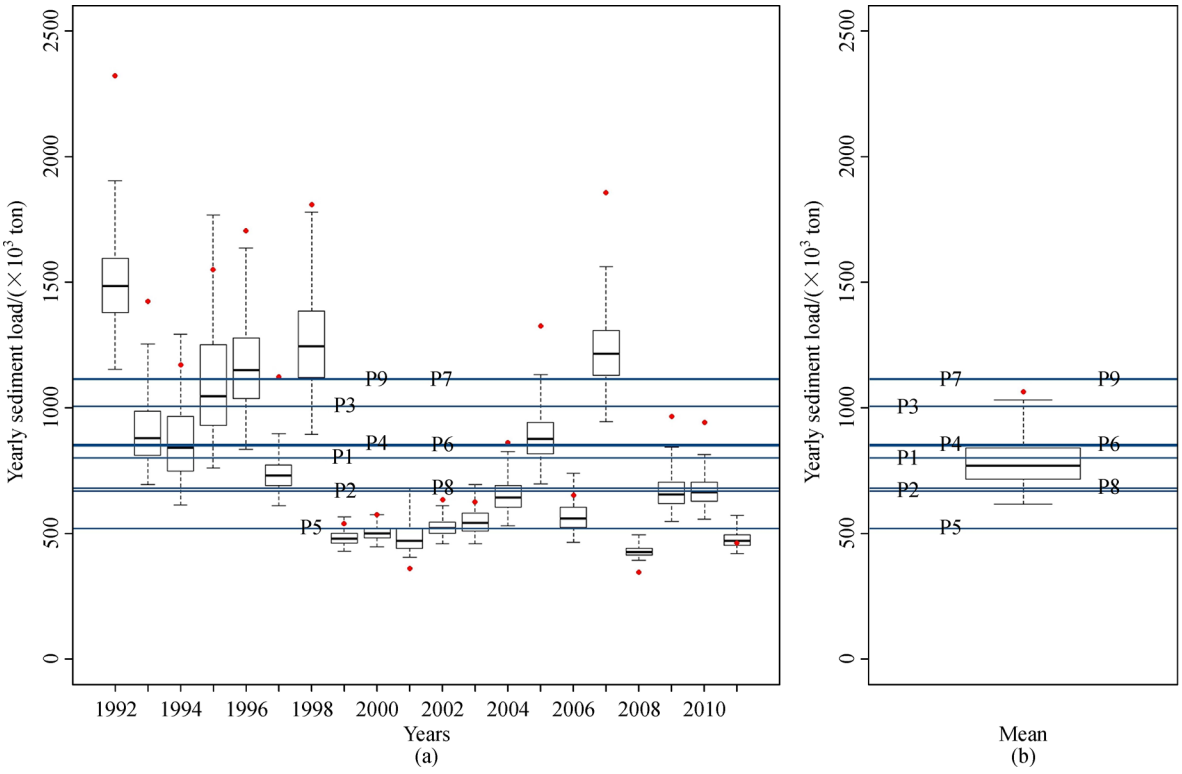

Fig. 10 (a) Yearly SSL for Shirgah-Talar station, (b) results compared with mean yearly sediment.

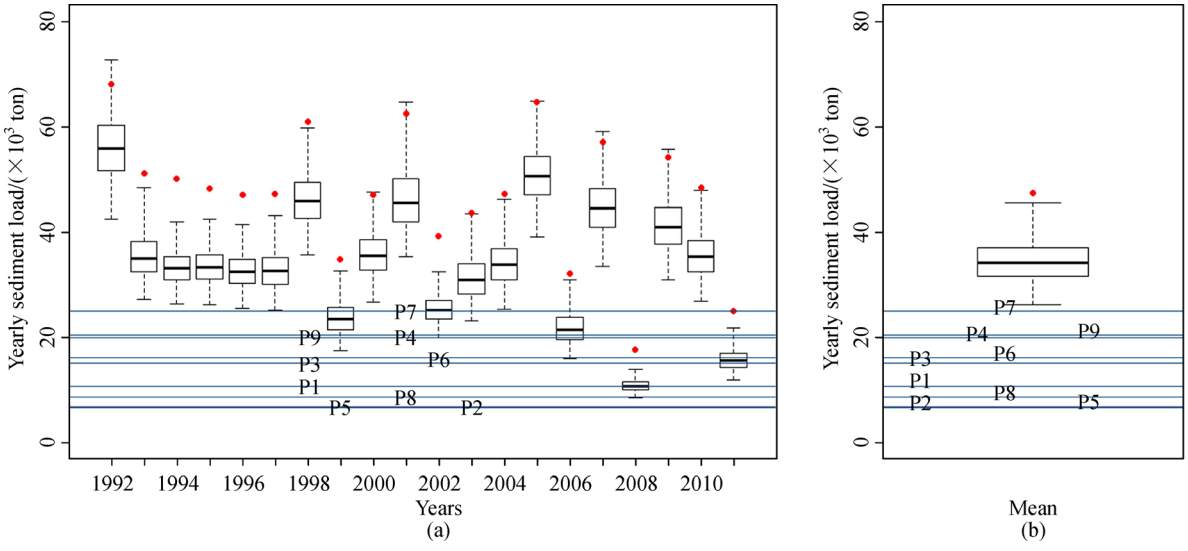

Fig. 11 (a) Yearly SSL for Valikbon station, (b) results compared with mean yearly sediment.

with USDA 703 method as the sub-factors to produce the *C* map in this method were similar to the USDA method. Yearly suspended sediment values obtained by the QR method and the least squares method in each year revealed high uncertainty in the estimation of the yearly SSL and substantial divergence of the results. In general, according to the results of delivered sediment by the SEDD model and the results of the SRC method, it can be concluded that P1 has the best performance. This procedure uses 15 min rainfall data to produce the rainfall-runoff erosivity factor. Further, the determination of *C* factor in this procedure was based on the land-use maps with assigning *C* factor values for each land-use class. Then, this procedure can be applied in watersheds with available 15 min rainfall data and utilizing satellite images.

References

Beven K, Kirkby M J (1979). A physically based, variable contributing area model of basin hydrology. Hydrol Sci J, 24(1): 43–69

Dai Z, Fagherazzi S, Mei X, Gao J (2016). Decline in suspended sediment concentration delivered by the Changjiang (Yangtze) River into the East China Sea between 1956 and 2013. Geomorphology, 268: 123–132

Dai Z, Liu J T, Wei W, Chen J (2015). Detection of the Three Gorges Dam influence on the Changjiang (Yangtze River) submerged delta. Sci Rep, 4(1): 6600 .

Dregne H E (1992). Erosion and soil productivity in Asia. J Soil Water Conserv, 47: 8–13

Eedy W (1995). The use of GIS in environmental assessment. Impact Assessment, 13(2): 199–206

Fathizad H, Karimi H, Alibakhshi S M (2014). The estimation of erosion and sediment by using the RUSLE model and RS and GIS techniques (case study: Arid and semi-arid regions of Doviraj, Ilam province, Iran). Int J Agric Crop Sci, 7: 303

Fernández C, Vega J A (2016). Evaluation of RUSLE and PESERA models for predicting soil erosion losses in the first year after wildfire in NW Spain. Geoderma, 273: 64–72

Ferro V, Minacapilli M (1995). Sediment delivery processes at basin scale. Hydrol Sci J, 40(6): 703–717

Ferro V, Porto P (2000). Sediment delivery distributed (SEDD) model. J Hydrol Eng, 5(4): 411–422

Fournier F (1960) Climate and erosion: the relationship between soil erosion by water and atmospheric precipitation. Dissertation for the Doctoral Degree. Paris: University of France

Hassan M, Roberge L, Church M, More M, Donner S, Leach J, Ali K (2017). What are the contemporary sources of sediment in the Mississippi River? Geophys Res Lett, 44(17): 8919–8924

Iikhchi A A, Hajabbassi M, Jalalian A (2003). Effects of converting range to dry-farming land on runoff and soil loss and quality in Dorahan, Chaharmahal & Bakhtiari Province. JWSS-Isfahan University of Technology, 6(4): 103–115

Koenker R (2012) Quantreg: Quantile Regression. R package version 4.98

Koenker R, Bassett G (1978) Regression quantiles. Econometrica, 46: 33–50

Lee S E, Kang S H (2014). Geographic information system-coupling sediment delivery distributed modeling based on observed data. Water Sci Technol, 70(3): 495–501

Mei X, Dai Z, Darby S E, Gao S, Wang J, Jiang W (2018). Modulation of extreme flood levels by impoundment significantly offset by floodplain loss downstream of the Three Gorges Dam. Geophys Res Lett, 45(7): 3147–3155

Minacapilli M, Santoro M (2003) Calibrating the SEDD model for Sicilian ungauged basins. Erosion Prediction in Ungauged Basins: Integrating Methods and Techniques, 279: 151

Mirakhorlo M S, Rahimzadegan M (2018). Application of sediment rating curves to evaluate efficiency of EPM and MPSIAC using RS and GIS. Environ Earth Sci, 77(20): 723

Mondal A, Khare D, Kundu S (2018). A comparative study of soil erosion modelling by MMF, USLE and RUSLE. Geocarto Int, 33(1): 89–103

Morgan R P C, Nearing M (2016). Handbook of Erosion Modelling. London: John Wiley & Sons

Renard KG, Foster GR, Weesies G, McCool D, Yoder D (1997) Predicting Soil Erosion by Water: a Guide to Conservation Planning with the Revised Universal Soil Loss Equation (RUSLE). Washington D C: US Department of Agriculture, Agricultural Research Service Washington

Renard KG, Freimund JR (1994) Using monthly precipitation data to estimate the *R*-factor in the revised USLE. J Hydrol (Amst), 157: 287–306

Riley S J, DeGloria S D, Elliot R (1999). A terrain ruggedness index that quantifies topographic heterogeneity. Intermt J Sci, 5: 23–27

Shiau J T, Chen T J (2015). Quantile regression-based probabilistic estimation scheme for daily and annual suspended sediment loads. Water Resour Manage, 29(8): 2805–2818

Tanyaş H, Kolat Ç, Süzen M L (2015). A new approach to estimate cover-management factor of RUSLE and validation of RUSLE model in the watershed of Kartalkaya Dam. J Hydrol (Amst), 528: 584–598

Van der Knijff J, Jones R, Montanarella L (2000). Soil erosion risk assessment in Europe. European Soil Bureau, European Commission Belgium.

Vrieling A (2006) Satellite remote sensing for water erosion assessment: a review. Catena, 65: 2–18

Wei L, Kinouchi T, Velleux M L, Omata T, Takahashi K, Araya M (2017). Soil erosion and transport simulation and critical erosion area identification in a headwater catchment contaminated by the Fukushima nuclear accident. J Hydro-environment Res, 17: 18–29

Wischmeier W H, Smith D D (1978). Predicting rainfall erosion losses—a guide to conservation planning. USDA, Science and Education Administration

Yang M, Li X, Hu Y, He X (2012) Assessing effects of landscape pattern on sediment yield using sediment delivery distributed model and a landscape indicator. Ecol Indic, 22: 38–52

Zounemat-Kermani M, Kişi Ö, Adamowski J, Ramezani-Charmahineh A (2016). Evaluation of data driven models for river suspended sediment concentration modeling. J Hydrol (Amst), 535: 457–472